3-D reconstruction of an axisymmetric flame based on cone-beam tomographic algorithms

Yuting He[1], Gang Lu[2], Yong Yan[2,1]
[1]School of Control and Computer Engineering, North China Electric Power University, Beijing, China
[2]School of Engineering and Digital Arts, University of Kent, Kent CT2 7NT, UK
hyt1220@foxmail.com, g.lu@kent.ac.uk, y.yan@kent.ac.uk*

Abstract— **This paper presents a method of 3-D (three-dimensional) reconstruction of an axisymmetric flame based on cone-beam tomographic algorithms. A FDK-based analytic tomographic algorithm is developed. Computer simulations are undertaken to evaluate the structural similarity between the template and the reconstructed volume so as to evaluate the effectiveness of the algorithm developed. Experimental tests were also conducted using a CCD camera to capture images of a candle flame. The 3-D reconstruction of the flame is then performed. The simulation and experimental results demonstrate the feasibility of the proposed cone-beam based tomographic algorithm for 3-D flame image reconstruction.**

Keywords− 3-D cone-beam tomography; reconstruction; axisymmetric flame; FDK-based algorithm

I. INTRODUCTION

3-D (three-dimensional) monitoring and characterization of burner flames is a key issue in the optimization of a combustion process. CT (Computed Tomography) techniques have been widely used in the medical industry for many decades and are increasingly adopted for various industrial applications. The tomographic techniques for the 3-D flame reconstruction can generally be classified into three categories, passive optical tomography, laser based tomography, and electrical tomography [1]. Among these methods, passive optical tomography uses the radiative information of the flame to reconstruct the flame luminosity and temperature if two-colour pyrometry is applied [2]. Both single- and multi-camera based approaches are proposed for monitoring laboratory and semi-industry scale burner flames [3-4]. The latter is superior to the former as more projections mean a higher spatial resolution of the reconstructed flame. A multi-camera system is also capable of reconstructing an unsteady or asymmetric flame. However, the single-camera system has obvious advantages over the multi-camera arrangement, including simple system setup, low capital cost and fast system response, making it especially useful in practical applications to industrial combustion systems.

On the other hand, in most passive optical tomographic systems there is a problem to be tackled, namely, the inconsistency between the optical set-up and mathematical model. In terms of reconstruction algorithms, the conventional algorithms, such as Filtered Back Projection (FBP) or Algebraic Reconstruction Technique (ART), are based on the assumption of parallel projections, i.e., pixel's rays are assumed to be parallel to the optical axis of a particular view. Ishino and Ohiwa [5] proposed the parallel-beam projection technique which was assumed that the flame size was negligible compared to the distance between the flame and lenses. Hossain et al [6] proposed a tomographic algorithm which combined the logical filtered back-projection (LFBP) and simultaneous algebraic reconstruction technique (SART) and was capable of performing 3-D flame reconstruction using only eight projections based on parallel-beam assumption. The method was evaluated using orthographic imaging templates and lab-scale burner flames. It was proved that the normalized radial error decreased with the objective distance and reached an error of less than 2% when the objective distance was 210 mm or greater. Anikin et al. [7] used ten telescopes which were arranged equidistantly from each other around the flame. An iris aperture positioned at the focal plane of the objective lens of the telescope was used to ensure that only parallel rays could pass the lens system. Wang et al [8] also proposed a multi-directional tomographic system. By analyzing the object points beyond the focal plane, an improved accuracy of the tomographic reconstruction was achieved. In many practical cases, however, the flame projections are generally formed by stacked fan-beams [9-11] or cone-beams [12, 13]. The assumption of the parallel-beams will result in a reduced accuracy in the flame reconstruction, particularly for the flame area which is away from the optical axis.

The present study is concerned with a tomographic method which is capable of performing the accurate 3-D reconstruction of axisymmetric flames using a single camera and the FDK cone-beam projection algorithm [14, 15]. The FDK algorithm is proposed by Feldkamp, Davis and Kress in 1984 [14]. The cone-beam projections are received by detector and stored in several 2-D matrices and every matrix relates to a projection view. By projecting the whole volume of the flame in one step, the reconstruction of flame regions which are away from the object central slice is achieved. The advantages of the proposed method include simple system setup, fast reconstruction process, and improved reconstruction accuracy. Both simulation and experimental results are presented and discussed.

II. METHODOLOGY

A. Generation of Projections

The 3-D cone-beam tomography includes projection acquisition and reconstruction of the volume data using acquired projections. Fig. 1 shows the flow chart of the generation of projections for the 3-D tomographic reconstruction of the flame.

- The first step is to define the simulation parameters which include, The voxel numbers of the template, i.e., the numbers of rows, columns and the piles of the 3-D template matrix;
- The pixel numbers of detector, i.e., the numbers of rows and columns of the 2-D detector matrix;
- The distance between the template center and the detector center;
- The number and range of projections, i.e., 180 projections received from 0-180°;

In the step "Calculating the contribution of every voxel of template to pixel of detector" (Fig. 1), the contribution can be calculated as [11],

$$\text{Ratio} = 1 - \frac{D_{td}}{D_{TD}}, \tag{1}$$

where D_{td} is the distance between a voxel in the template and a pixel in the camera sensor plane and D_{TD} is the distance between the distant side of the template and the camera sensor plane.

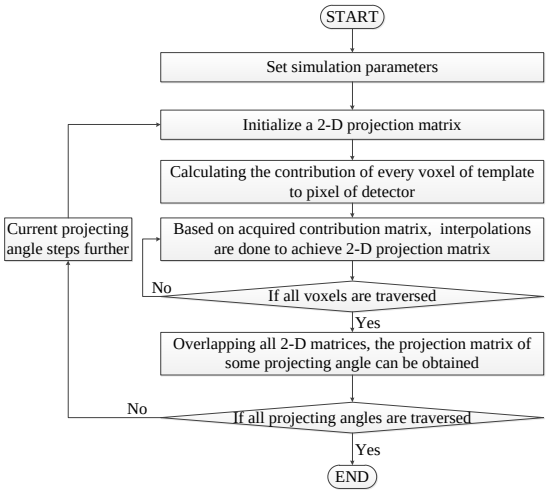

Figure 1. Flow chart of the generation of flame projections.

B. FDK-based Reconstruction Algorithm

Compared to iterative methods, analytic methods have advantages of high reconstruction speed and easy implementation in common software tools such as Matlab. The FDK algorithm is the fast representative of analytic methods and also a development of the 2-D fan-beam FBP[16]. Since the whole template can be projected in one step using the cone-beam projection structure and the analytic method can directly reconstruct the template, the FDK-based reconstruction algorithm is faster.

The algorithm used in this study is based on the FDK algorithm. The 'cone-beam' is the cone of rays passing through the flame and meeting at the optical center of the imaging lens, and terminating on the individual pixels of the CCD camera sensor plane.

The reconstruction procedure consists of three steps:

1) Weighting the Projecting Data.

$$\omega(p,z) = \frac{D_{CF}}{\sqrt{D_{CF}^2 + p^2 + z^2}}, \tag{2}$$

$$\tilde{R}_\beta(p,z) = \omega R_\beta(p,z), \tag{3}$$

where D_{CF} is the distance between the cone point and the flame, (p, z) is the camera coordinate system, ω(p,z) is the weight of projecting data calculated according to the location of the flame and the camera. R_β(p, z) is the cone-beam projection of the imaging sensor plane received at angle β (i.e., the rotation angle of the flame coordinate system around the z-axis) and $\tilde{R}_\beta$(p, z) is the weighted projecting data. Because the size of the flame is much larger than the camera imaging sensor , the distance between the lens focal point and the camera sensor plane is incomparable to that between the flame and the camera sensor plane. Therefore, projections are assumed focusing on the camera sensor plane, and thus the "cone-beam" actually starts from the camera imaging sensor plane.

2) Filtering Each Row of Whole Projections.

$$\hat{R}_\beta(p,z) = \tilde{R}_\beta(p,z) h\left(\frac{D_{CF} t}{D_{CF} - s} - p\right), \tag{4}$$

where (t, s, z) is the rotated coordinate system of the flame, h(.) is the ordinary filter, $\hat{R}_\beta$(p, z) is the filtered projecting data.

3) Performing Cone-beam Back Projection of the Filtered Projections.

$$f(t,s,z) = \frac{1}{2}\int_0^{2\pi} \frac{D_{CF}}{(D_{CF} - s)^2} \int_{-\infty}^{\infty} \hat{R}_\beta(p,z)\, dp\, d\beta, \tag{5}$$

where f(t,s,z) is the reconstructed volume data.

So combining equations (2), (3), (4) and (5), (6) can be derived as follows,

$$f(t,s,z) = \frac{1}{2}\int_0^{2\pi} \frac{D_{CF}}{(D_{CF} - s)^2} \int_{-\infty}^{\infty} R_\beta(p,z) h\left(\frac{D_{CF} t}{D_{CF} - s} - p\right) \frac{D_{CF}}{\sqrt{D_{CF}^2 + p^2 + z^2}}\, dp\, d\beta, \tag{6}$$

With the increase of β from 0 to 2π, all projections are filtered-back projected to the volume.

III. Results and Discussions

A. Computer Simulation

The internal structure of a burner flame is very complex. Initial studies are conducted to simulate and evaluate the effectiveness of the proposed 3-D cone-beam tomographic algorithm in the reconstruction of a flame-like template. As shown in Fig. 2, the template consists of several circle slices with varied gray-scales, i.e., the gray-level in outer regions is lower than inner regions. These circles have different diameters to simulate the shape and size of the flame. Assuming that the size of each pixel in the template is 1 mm, the template is 50 mm high and the radius of its maximum circle is 25mm.

By adjusting the value of D_{CF}, different distances between the flame and the camera are simulated. In this study, five flame sections are chosen in the horizontal and vertical directions, respectively. TABLES I and II show the reconstructed images in comparison with the corresponding original template from horizontal and vertical perspectives. The cross-sections move along the z-axis and the longitudinal-sections move along the x-axis.

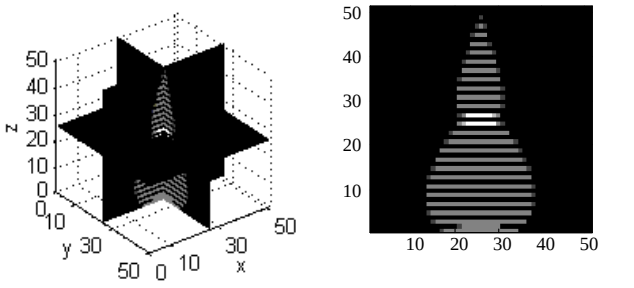

(a) 3-D visualization of the flame-like template

(b) Y-Z view of the flame-like template

Figure 2. An example of the flame-like template.

TABLE I. Reconstructed Cross-sections (z-axis) of the Flame-like Template for Different D_{CF}s.

D_{CF} (mm) \ z-axis (mm)	9	17	25	33	41
155	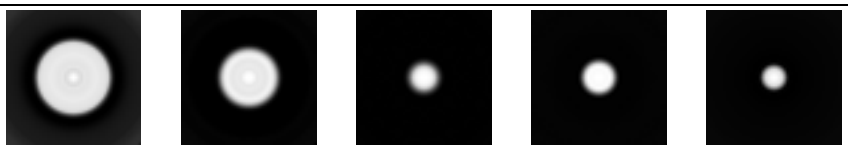				
175	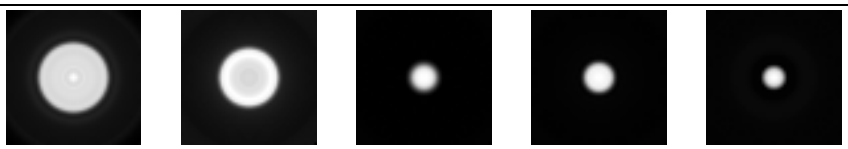				
195	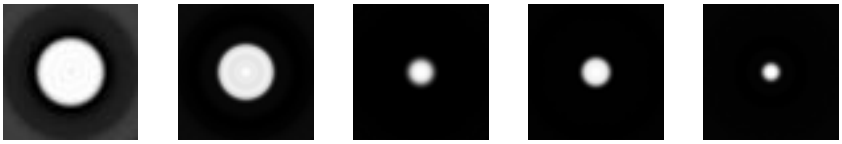				
∞(template)					

TABLE II. RECONSTRUCTED LONGITUDINAL-SECTIONS (X-AXIS) OF THE FLAME-LIKE TEMPLATE FOR DIFFERENT D_{CF}S.

D_{CF} (mm) \ x-axis (mm)	17	21	25	29	33
155					
175					
195					
∞(template)	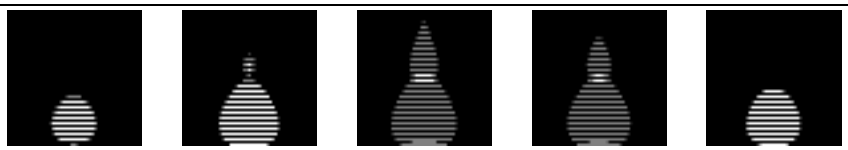				

As can be seen from TABLES I and II, for all cross- and longitudinal-sections, the reconstructed images tend to be more similar to the template when the value of D_{CF} increases. This phenomenon can be interpreted by the fact that, with the increase in the distance between the template and the detector, the projection rays tend to be in parallel, which is the case most parallel-beam tomographic models are based on, as a result, the reconstruction is more accurate.

In addition, the computer used in this work is i5-460M (2.53GHz), 4G RAM, Win7 Pro32 with Matlab version R2014a. The processing time for the reconstruction of each section is only around 3.2s, indicating the proposed algorithm has a fast response time.

The reconstruction accuracy is evaluated with reference to the image structural similarity index (SSIM) [17]. The SSIM ranges from -1 to 1, and the closer to 1, the more similar the reconstructed image to the template. The calculation of the SSIM has three aspects, i.e., luminance, contrast and structure, which are obtained as follows,

$$\mathrm{SSIM}(x,y) = [l(x,y)]^{\alpha} \cdot [c(x,y)]^{\beta} \cdot [s(x,y)]^{\gamma}, \tag{7}$$

and,

$$l(x,y) = \frac{2\mu_x\mu_y + C_1}{\mu_x^2 + \mu_y^2 + C_1}, \tag{8}$$

$$c(x,y) = \frac{2\sigma_x\sigma_y + C_2}{\sigma_x^2 + \sigma_y^2 + C_2}, \tag{9}$$

$$s(x,y) = \frac{\sigma_{xy} + C_3}{\sigma_x\sigma_y + C_3}. \tag{10}$$

For the template and the reconstructed image, where μ_x and μ_y are their local means, σ_x and σ_y are their standard deviations, and σ_{xy} is the cross-covariance between them. Generally, the default value of α, β and γ are all 1. C1, C2 and C3 are constants to keep stability and can be calculated from the following equations,

$$C_1 = (k_1 L)^2, \tag{11}$$

$$C_2 = (k_2 L)^2, \tag{12}$$

$$C_3 = \frac{C_2}{2}, \tag{13}$$

where k_1 is 0.01 and k_2 is 0.03, generally, and L is the dynamic range of the pixel values.

Fig. 3 illustrates the results of the SSIM for evaluating the similarity between the original template and the reconstructed image.

As can be seen in Fig. 3(a), although the SSIMs show a similar trend for all z, it varies with z, especially for z=9 and z=17. These two sections have larger outlines, particularly section z=9 is furthest from the central plane among all cross-sections. Fig. 3(b) show that section x=25 has the maximum SSIM due to the fact that this section is the closest section to the central plane. The other two sets of sections: x=21, x=29 and x=17, x=33 have shown a similar SSIM.

It is noted that the SSIMs illustrated in Fig. 3 share common characteristics. Every single curve, especially in Fig. 3(b), experiences a very similar trend, which looks like the curve of "arctan(x)". In the initial stage, the SSIM is a concave function, which demonstrates the effectiveness of the cone-beam based algorithm in tackling the problem of the distortion happened in a small D_{CF}. In the end stage, the SSIM seems to be stable owing to the parallel projections approximation in a large D_{CF}.

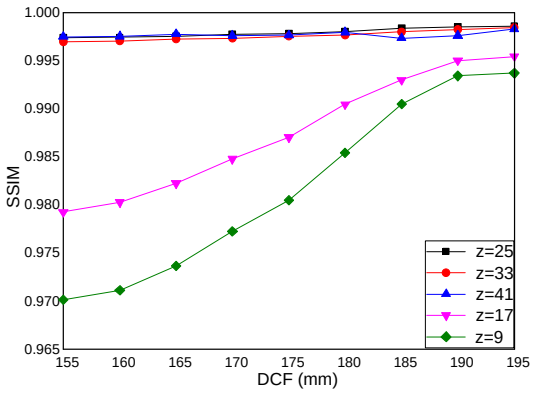

(a) SSIM of five reconstructed cross-sections.

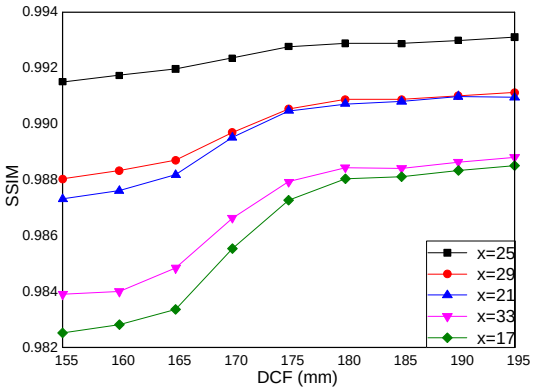

(b) SSIM of five reconstructed longitudinal-sections.

Figure 3. SSIM of 10 flame sections.

B. Experimental Results

To evaluate the performance of the proposed algorithm, experiments were conducted on a laboratory-scale combustion test rig. In general, the acquisition of flame projections should be done more than one view for the tomographic reconstruction. the present study focuses, however, on tackling the inconsistency problem between the optical set-up and the reconstruction model, and thus only a single camera is used to capture the images of a rotationally symmetric flame, i.e., a candle flame in this case. Fig. 4 shows the experimental set-up. The camera used is a megapixel USB2.0 CCD monochromatic camera which has pixels of 1296×964. The camera equipped with a close-up zoom lens with the focal length ranging from 13-130 mm and the zoom ratio of 10:1. During the image acquisition, the frame rate of the camera was set to be 30 fps and the shutter speed was 33.328 ms (set in the camera software). The 2-D images of the flame were captured for different distances between the flame and the camera. A total of 60 images were captured under a stable condition at each distance, which were then used for reconstruction. A gray-threshold segmentation was employed to remove the noise of image background. Fig. 5(a) is the original 2-D images of the flame obtained. The images were then used to reconstruct the flame based on the cone-beam algorithm as described in Section II.

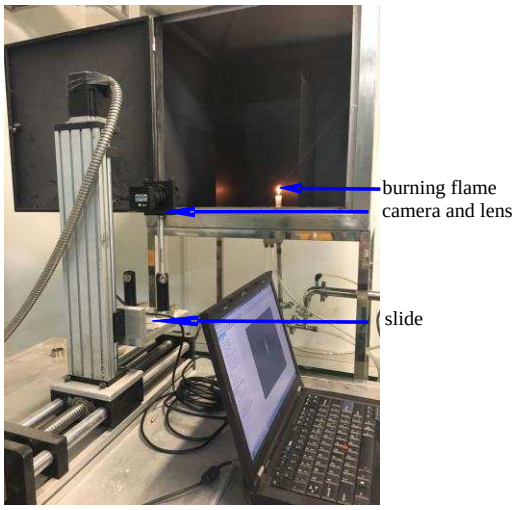

Figure 4. Experimental set-up.

Fig. 5(b) illustrates the reconstructed longitudinal central sections of the flame based on the captured 2-D images, whilst Fig. 6 shows the reconstructed cross-sections. In this study, 3 sections in each direction are chosen to be representatives. As can be seen from the reconstruction results, the proposed method is capable of reconstructing the in-situ flame accurately, not only the gray level but also the inner structure. In addition, the color images shown in Fig. 5(b) illustrate the luminous levels of the captured flame, which is consistent with our common sense. In other words, the luminance is higher in red regions, which locates in outer flame and is lower in blue regions, which are inner flame.

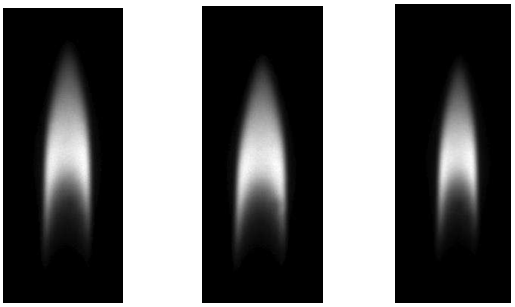

270 mm 370 mm 470 mm

(a) Flame images captured from 3 different distances.

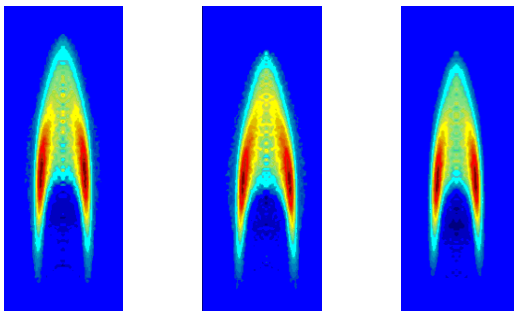

270mm 370mm 470mm

(b) Reconstructed central sections of the flame corresponding to (a).

Figure 5. Flame images and reconstructed central sections.

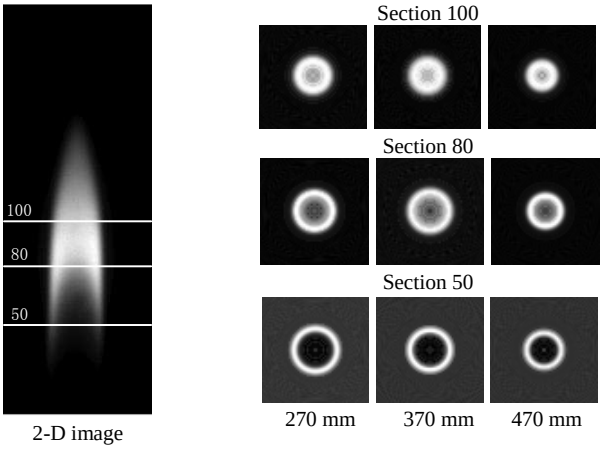

Figure 6. Reconstructed cross-sections for 3 different distances.

IV. CONCLUSIONS

A cone-beam tomographic method for the 3-D reconstruction of rotationally symmetric flames has been proposed to tackle the non-parallel problem which is associated with 3-D flame reconstruction algorithms. Benefiting from the fast and cone-beam based characteristics of FDK algorithm, a FDK-based algorithm is proposed to reconstruct flame image. Computer simulations have been undertaken to evaluate the structural similarity between the template and the reconstructed volume. Experimental results obtained on a lab-scale combustion rig have also demonstrated that the proposed cone-beam based tomographic algorithms is capable of performing 3-D flame reconstruction with a better accuracy and system response, especially in the regions which are further away from the optical center of the flame.

REFERENCES

[1] Y. Yan, T. Qiu, G. Lu, Md. Moinul Hossain, G. Gilabert and S. Liu, "Recent advances in flame tomography," Chinese Journal of Chemical Engineering, vol. 20, no. 2, pp. 389-399, 2012.

[2] H. J. Wang, Z. F. Huang, D. D. Wang, et al, "Measurements on flame temperature and its 3D distribution in a 660 MWe arch-fired coal combustion furnace by visible image processing and verification by using an infrared pyrometer," Measurement Science and Technology, vol. 20, no. 11, pp. 114006, 2009.

[3] Q. X. Huang, F. Wang, D. Liu, et al, "Reconstruction of soot temperature and volume fraction profiles of an asymmetric flame using stereoscopic tomography," Combustion and Flame, vol. 156, no. 3, pp. 565-573, 2009.

[4] G. Gilabert, G. Lu and Y. Yan, "Three-dimensional tomographic reconstruction of the luminosity distribution of a combustion flame", IEEE Transactions on Instrumentation and Measurement, vol. 56, no. 4, pp. 1300-1306, 2007.

[5] Y. Ishino and N. Ohiwa, "Three-dimensional computerized tomographic reconstruction of instantaneous distribution of chemiluminescence of a turbulent premixed flame," JSME International Journal Series B, vol. 48, no. 1, pp. 34-40, 2005.

[6] M. M. Hossain, G. Lu and Y. Yan, "Optical fiber imaging based tomographic reconstruction of burner flames," IEEE Trans. Instrum. Meas., vol. 61, no. 5, pp. 1417-1425, 2012.

[7] N. Anikin, R. Suntz and H. Bockhorn, "Tomographic reconstruction of the OH*-chemiluminescence distribution in premixed and diffusion flames," Applied Physics B, vol. 100, no. 3, pp. 675-694, 2010.

[8] J. Wang, Y. Song, Z. H. Li, A. Kempf and A. Z. He, "Multi-directional 3D flame chemiluminescence tomography based on lens imaging," Optics letters, vol. 40, no. 7, pp. 1231-1234, 2015.

[9] E. J. Beiting, "Fiber-optic fan-beam absorption tomography," Applied optics, vol. 31, no. 9, pp. 1328-1343, 1992.

[10] J. Lim, Y. Sivathanu and D. Feikema, "Fan beam emission tomography for estimating scalar properties in laminar flames," Third Joint Meeting of the US Sections of the Combustion InstituteNASA, Chicago, Illinois, pp. 1–6, 2003.

[11] K. E. Bennett, G. W. Faris and R. L. Byer, "Experimental optical fan beam tomography," Applied optics, vol. 23, no. 16, pp. 2678-2685, 1984.

[12] J. Floyd, P. Geipel and A. M. Kempf, "Computed tomography of chemiluminescence (CTC): instantaneous 3D measurements and phantom studies of a turbulent opposed jet flame," Combustion and Flame, vol. 158, no. 2, pp. 376-391, 2011.

[13] H. Zhao, B. Williams and R. Stone, "Measurement of the spatially distributed temperature and soot loadings in a laminar diffusion flame using a Cone-Beam Tomography technique," Journal of Quantitative Spectroscopy and Radiative Transfer, vol. 133, pp. 136–152, 2014.

[14] L. A. Feldkamp, L. C. Davis and J. W. Kress, "Practical cone-beam algorithm," JOSA A, vol. 1, no. 6, pp. 612-619, 1984.

[15] W. C. Scarfe and A. G. Farman, "What is cone-beam CT and how does it work?" Dental Clinics of North America, vol. 52, no. 4, pp. 707-730, 2008.

[16] T. M. Buzug, "Computed tomography: from photon statistics to modern cone-beam CT," Springer Science & Business Media, ISBN 978-3-540-39407-5, pp. 376, 2008.

[17] Z. Wang, A. C. Bovik, H. R. Sheik and E. P. Simoncelli,"Image quality assessment: from error visibility to structural similarity," IEEE transactions on image processing, vol. 13, no. 4, pp. 600-612, 2004.